Journal of Inorganic Biochemistry 149 (2015) 12–24

Contents lists available at ScienceDirect

Journal of Inorganic Biochemistry

journal homepage: www.elsevier.com/locate/jinorgbio

# Insights into the mechanisms underlying the antitumor activity of an oxidovanadium(IV) compound with the antioxidant naringenin. Albumin binding studies

María S. Islas [a], Luciana G. Naso [a], Luis Lezama [b,d], María Valcarcel [c], Clarisa Salado [c], Meritxell Roura-Ferrer [c], Evelina G. Ferrer [a], Patricia A.M. Williams [a,*]

[a] Centro de Química Inorgánica (CEQUINOR, CONICET, UNLP), Departamento de Química, Facultad de Ciencias Exactas, Universidad Nacional de La Plata, 47 y 115-C.C.962-B1900AVV, 1900 La Plata, Argentina
[b] Departamento de Química Inorgánica, Facultad de Ciencia y Tecnología, Universidad del País Vasco UPV/EHU, P.O. Box 644, 48080 Bilbao, Spain
[c] Innoprot SL, Parque científico y Tecnológico de Bizkaia, Edificio 502-P1, 48160 Derio, Spain
[d] BCMaterials, Parque científico y Tecnológico de Bizkaia, Edificio 500-1, 48160 Derio, Spain

ARTICLE INFO

*Article history:*
Received 23 February 2015
Received in revised form 17 April 2015
Accepted 19 April 2015
Available online 25 April 2015

*Keywords:*
Oxidovanadium(IV) complexes
Naringenin
Antioxidant properties
Mechanism cytotoxic action
BSA binding

ABSTRACT

Naringenin, a natural antioxidant present in grapefruit, oranges and the skin of tomatoes showed low antioxidant properties among other flavonoids due to its structural characteristics. Since many flavonoids were shown to have cell-killing and antioxidant activities, naringenin was investigated herein. In parallel with its antioxidant activities the flavonoid showed very low cytotoxicity at concentrations up to 100 μM against lung (A549) and breast (SKBr3 and MDAMB231) cancer cell lines. Furthermore, a newly-synthesized and characterized complex of naringenin and oxidovanadium(IV) ($[V^{IV}O(nar)_2]\cdot 2H_2O$, VOnar, with weak ferromagnetic coupling) was also studied. As a result, VOnar acted as a better compound on cell-killing and antioxidant activities (*in vitro*) than naringenin. The anti-proliferative effect of VOnar was accompanied by reactive oxygen species (ROS) generation, cell membrane and DNA damages, cell cycle arrest, caspase 3/7 activation and mitochondrial potential reduction. The higher parameters observed for the MDAMB231 cell line have been related to its low glutathione (GSH) content. The assays of the interaction of bovine serum albumin (BSA) with the complex showed the affinity of protein toward it and that there is only one binding site on the BSA molecule. However, metal complexation decreased the binding affinity to BSA of naringenin probably due to a steric hindrance of the complex.


## 1. Introduction

The phytochemical flavonoids have been extensively investigated over the years due to their benefit from their medicinal and pharmacological properties. In addition to their well known antioxidant properties, flavonoids have been reported to possess anticancer, antiinflammatory, antiatherosclerotic and antiviral activities [1]. Flavonoids in combination with anticancer agents have been found to enhance cancer chemotherapy [2]. In recent years owing to their chelating properties the structure of flavonoids has been modified by metal ion complexation and their biological properties have been improved [1]. The metal ions interacted most likely with the keto and hydroxyl groups of the flavonol skeleton (see Fig. 1) and for flavonoid O-glycosides that possess sugars bound to the OH groups, the metal ions can interact through the OH groups of the glycones according to the experimental conditions employed during their synthesis [3]. In many of these metal complexes the biological properties of the flavonoids were enhanced and then new antitumoral and antioxidant agents were produced.

Naringenin (nar), 4′,5,7-trihydroxyflavanone, can be found in grapefruit, oranges and tomatoes, Fig. 1 [4]. The flavonoid and its metal complexes are considered to have biological effects as antioxidant, antiinflammatory and antitumoral [5–7]. For instance, the copper complex of naringenin enhanced the inhibitory rate of the ligand against HepG2 cell lines in a relatively significant mode [8]. On the other side, vanadium, an ultra trace nutrient, is an essential metal present in the active sites of some enzymes that have influences on cellular growth and their oxidation–reduction processes which deserve increasing attention for application to biomedical sciences. An intensive search for vanadium complexes as therapeutic agents with insulin mimetic and antitumor properties is being actively developed. Many of the vanadium compounds proposed for the use against diabetes have shown cytotoxic effects against tumor cell lines [9]. In order to obtain vanadium complexes with antitumor properties we have synthesized and studied different flavonoid–metal complexes with oxidovanadium(IV) cation [10]. In general, the antitumor effect of these compounds has been attributed to apoptotic effects. To determine the relationship between

* Corresponding author. Tel./fax: +54 221 4259485.
*E-mail address:* williams@quimica.unlp.edu.ar (P.A.M. Williams).

http://dx.doi.org/10.1016/j.jinorgbio.2015.04.011
0162-0134/

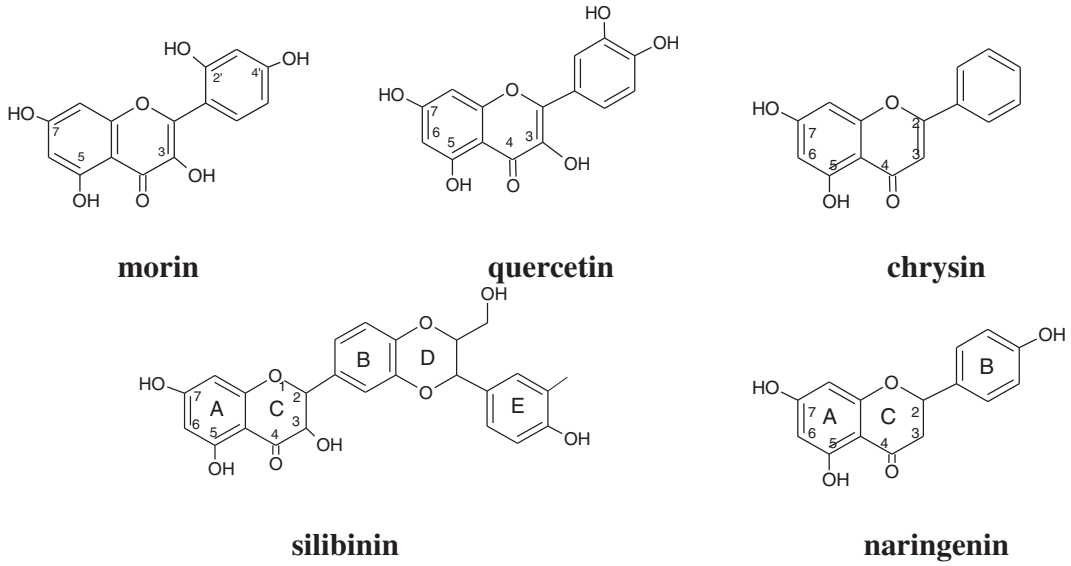


**Fig. 1.** Structures of selected flavonoids: naringenin, chrysin, morin, quercetin and silibinin.

the structure of VOflavonoid complex and biological activities, we have selected the flavonoid naringenin that allows direct comparisons with the behavior of the oxidovanadium(IV) complexes previously reported with chrysin, silibinin, morin and quercetin Fig. 1 [11–14].

The new complex, $[V^{IV}O(nar)_2]\cdot 2H_2O$, has been characterized by elemental analysis, UV–visible (UV–vis), diffuse reflectance, FTIR and EPR spectroscopies and magnetic and thermogravimetric determinations. The antioxidant determinations confirmed that naringenin possesses low antioxidant properties than quercetin (one of the strong antioxidant flavonoids, with a similar structure and also containing C2 = C3 double bond and 3-OH and 3′-OH groups) but an enhancement of the radical scavenging properties has been found upon complexation. Since many flavonoids were reported to show cell-killing activity, naringenin was investigated herein for these activities. Furthermore, the newly-synthesized complex VOnar was also studied. Low antitumoral effects have been found for naringenin (up to 100 μM concentration) in lung cancer A549 and breast cancer SKBr3 and MDAMB231 cell lines, according to the low antioxidant power. The complexation enhanced the cytotoxicity and, for the breast cancer cells with high growth inhibitory effects, an apoptotic mechanism of action could be determined by means of oxidative stress with DNA damage and loss of the plasmatic and mitochondrial membrane integrities, caspase 3/7 activation and mitotic arrest. The higher parameters obtained for these effects on MDAMB231 cell lines in relation to the SKBr3 cell line have been associated with the low antioxidant machinery (GSH contents) in the first cell line. The complexation decreased the binding affinity to bovine serum albumin (BSA) of naringenin probably due to a steric hindrance of the complex.

## 2. Experimental

### 2.1. Materials and measurements

All reagents and chemicals were purchased from commercial sources and used as received. Elemental analysis for carbon and hydrogen was performed using a Carlo Erba EA1108 analyzer. Vanadium content was determined by tungstophosphovanadic method [15]. Thermogravimetric (TG) analysis and differential thermal analysis (DTA) were performed with Shimadzu systems (models TG-50 and DTA-50, respectively), working in an oxygen flow of 50 mL $min^{-1}$ and at a heating rate of 10 °C $min^{-1}$. Sample quantities ranged between 10 and 20 mg. $Al_2O_3$ was used as a differential thermal analysis standard. UV–vis spectra determinations were recorded with a Hewlett-Packard 8453 diode-array spectrophotometer. The diffuse reflectance spectrum was recorded with a Shimadzu UV-300 spectrophotometer, using MgO as a standard. Infrared spectra were measured with a Bruker IFS 66 FTIR spectrophotometer from 4000 to 400 $cm^{-1}$ using the KBr pellet technique. A Bruker ESP300 spectrometer operating at the X-band and equipped with standard Oxford Instruments low-temperature devices (ESR900/ITC4) was used to record the spectrum of the complex at room temperature in the solid state. A computer simulation of the EPR spectra was performed using the program WINEPR SimFonia (version 1.25, Bruker Analytische Messtecnik, 1996). Magnetic susceptibility measurements on polycrystalline samples were performed in the temperature range 5–300 K with a Quantum Design MPMS-7 superconducting quantum interference device magnetometer and using an applied field of 0.1 T. Diamagnetic corrections of the constituent atoms were estimated from Pascal's constants. Fluorescence spectra were obtained using a Perkin Elmer (Beaconsfield, UK) LS-50B luminescence spectrometer equipped with a pulsed xenon lamp (half peak height less than 10 μs, 60 Hz), an R928 photomultiplier tube, and a computer working with FLWinlab.

### 2.2. Synthesis of $[V^{IV}O(nar)_2]\cdot 2H_2O$, VOnar

Naringenin was dissolved in absolute ethanol (0.5 mmol, 3 mL) and the pH was raised to 8 by the addition of a solution of ammonia (30% in water) in absolute ethanol ($NH_3$/EtOH). Then, a 50% aqueous solution of $VOCl_2\cdot 2H_2O$ (0.25 mmol, 500 μL) in absolute ethanol was added under continuous stirring and the pH of the green solution was adjusted to 8 with $NH_3$/EtOH. With the aim to prevent the oxidation reaction of naringenin with atmospheric oxygen, the entire synthesis was performed under nitrogen atmosphere. A green–yellow precipitate was formed by conjunction with the evaporation of ethanol caused by the flux of nitrogen at room temperature. The precipitate was filtered off, washed several times with water and dried in an oven at 60 °C. Anal. Calc. ($C_{30}H_{26}O_{13}V$): C: 55.7%; H: 4.0%; V: 7.9%; Exp: C: 55.6%; H: 4.0%; V: 7.8%. Thermogravimetric analysis confirmed the presence of two labile water molecules (Exp. loss: 5.6%. Calc. loss: 5.6%; broad endothermic peak, DTA, T 60 °C). At 800 °C the total weight loss (85.9%, calc; 86.1%, exp) was in agreement with the formation of $V_2O_5$, characterized by means of FTIR spectroscopy. UV–vis (abs. EtOH): 576 nm (14.2 $M^{-1}$ $cm^{-1}$), 680 nm, br (15.7 $M^{-1}$ $cm^{-1}$). Diffuse reflectance spectrum: 420 nm, 570 nm and 820 nm.

### 2.3. Antioxidant properties

The antioxidant properties were assayed following our reported methods [12]. The antiradical activity was determined from the reaction of naringenin and VOnar with a methanolic solution of 1,1-diphenyl-2-picrylhydrazyl (DPPH•). The trolox equivalent antioxidant capacity (TEAC) was calculated from the slope of the plot of the percentage inhibition of absorbance of $ABTS^{+}$•, generated by incubating ABTS (2,2′-azinobis(3-ethylbenzothiazoline-6-sulfonic acid) diammonium salt) with potassium persulfate, *versus* the concentration of the antioxidant divided by the slope of the plot for Trolox (6-hydroxy-2,5,7,8-tetramethylchroman-2-carboxylic acid). The superoxide dismutase (SOD) activity was examined indirectly using the ability of the compounds to inhibit the reduction of nitroblue tetrazolium (NBT) by superoxide anion generated by the phenazine methosulfate (PMS) and NADH system. The scavenging of the hydroxyl radical (generated by the ascorbate–iron–$H_2O_2$ system) was measured by the extent of the deoxyribose degradation generated by those radicals with the thiobarbituric acid method. Peroxyl radicals have been generated by the thermal decomposition of 2,2-azobis(2-amidinopropane) dihydrochloride (AAPH). Pyranine (trisodium 8-hydroxypyerene-1,3,6-trisulfonate) was consumed by these radicals. The delay of pyranine consumption (lag phase) by peroxyl radicals in the presence of the competitive antioxidants was calculated as the time before the consumption of pyranine started (notable reductions in absorbance).

### 2.4. Cell culture assays

Human lung cancer cell line A549 was obtained from ABAC (Argentinean Cell Bank Association INEVH, Pergamino, Buenos Aires, Argentina). Cells were maintained at 37 °C in a 5% carbon dioxide atmosphere using the following culture medium: DMEM supplemented with 100 U/mL penicillin, 100 μg/mL streptomycin and 10% (v/v) fetal bovine serum. When 70–80% confluence was reached, cells were subcultured using TrypLE™ from Gibco (Gaithersburg, MD, USA), free phosphate buffered saline (PBS) (11 mM $KH_2PO_4$, 26 mM $Na_2HPO_4$, 115 mM NaCl, pH 7.4). For the experiments, cells were grown in multi-well plates. When cells reached 70% confluence, the monolayers were washed twice with DMEM and then incubated with the different compounds.

Human MDAMB231 and SKBr3 breast cancer cell lines were obtained from HPA Culture Collection (Salisbury, United Kingdom). The first cell line was cultured in endotoxin-free RPMI medium supplemented with 10% fetal bovine serum (FBS), 1% non-essential amino acids and 100 U/mL penicillin and 100 μg/mL streptomycin. SKBr3 cells were cultured in endotoxin-free McCoy medium supplemented with 10% FBS and 100 U/mL penicillin and 100 μg/mL streptomycin. All reagents were from Sigma-Aldrich (St Louis, MO). Cultures were maintained at 37 °C in a humidified atmosphere with 5% $CO_2$ and passaged according to th manufacturer's instructions.

#### 2.4.1. Crystal violet assay

The compounds were dissolved in DMSO just before the experiment and a calculated amount of these solutions was added to the growth medium containing cells at a final solvent concentration of 0.5% which had no discernible effect on cell killing. The growth inhibitory effect toward the cancer A549 cell line was evaluated by means of the crystal violet bioassay. Briefly, $2.0 \times 10^4$ cells/well were seeded in 48-well microplates in growth medium (500 μL) and then incubated at 37 °C in a 5% carbon dioxide atmosphere. After 24 h, the medium was removed and replaced with a fresh one containing the compounds to be studied at the appropriate concentration. Triplicate cultures were established for each treatment. After 24 h, each well was treated with crystal violet and washed to remove the excess of dye. The crystal violet taken up by the cells was extracted with the buffer and the inhibition of cell growth induced by the tested compounds was detected by measuring the absorbance of each well at 540 nm. Mean absorbance for each drug dose was expressed as a percentage of the control untreated well absorbance and plotted *vs.* drug concentration.

#### 2.4.2. MTT (3-(4,5-dimethylthiazol-2-yl)-2,5diphenyltetrazolium bromide) assay

Breast cancer cells were seeded at a density of 5000/well in 96 well plates, grown overnight and treated with either vehicle, naringenin, VOnar or oxidovanadium(IV) of different concentrations in FBS free medium. The dissolution vehicle was dimethyl sulfoxide to yield a maximum final concentration of 0.5% in the treated well (Sigma-Aldrich, St. Louis, MO). After 24 h of incubation at 37 °C, MTT was added at 100 μg/well for 2 h (Sigma-Aldrich, St. Louis, MO). The formazan products generated by cellular reduction of MTT were dissolved in DMSO and the optical density was measured at 450 nm using synergy 2 multi-mode microplater reader Biotek (Winooski, USA). All experiments were done in triplicate.

#### 2.4.3. High content analysis image assay

For the high content analysis image assay the MDAMB231 and SKBr3 cells were seeded at a density of 5000/well in a collagen-coated 96 well plate and stained with fluorescent probes (Invitrogen, Life Technologies, Madrid, Spain) for 30 min. Tetramethyl rhodamine methyl ester (TMRM) 50 μM has been added for the measurement of mitochondrial depolarization related to cytosolic $Ca^{2+}$ transients, 2,7,dichlorodihydrofluorescein diacetate acetyl ester ($H_2$DFF-DA) 1 μM, for the measurement of reactive oxygen species (ROS) production and 5 μM CellEvent™ Caspase 3/7 Green Detection Reagent for the measurement of caspase 3/7 activation. After 30 min, cells were washed three times and treated with naringenin, VOnar and the oxidovanadium(IV) cation generated from the dissolution of $V^{iv}OSO_4$, for 24 h. The two probes were measured at 24 h and ROS localization was identified with an absorption/emission maxima of 488/530 (Ex/Em) nm while TMRM has been measured at 549/600 (Ex/Em) nm and CellEvent™ Caspase 3/7 Green Detection Reagent at 502/530 nm using the BD Pathway™ 20× Olympus Objective. The intracellular glutathione determination has been performed using monochlorobimane 10 μM during 30 min at 37 °C. Then, cells were washed 3 times and the fluorescence intensity (in cytoplasm) was measured at 345/425 (Ex/Em) nm. Data were analyzed choosing a region of interest (Text Overlay: ROI (regions-of-interest)) tool from the Attovision program to select the areas. Then, ROIs from the entire cell body, ROIs from mitochondrial regions or ROIs from nuclear regions in imaged cells were selected to measure the fluorescence intensities (Arbitrary Units-AU) of ROS, TMRM respectively. The average fluorescence intensities were calculated from all ROIs of each cell for each time point subtracting the background fluorescence intensity (regions next to cells). After the measurements with the probes, conditioned medium from each well was collected for lactate dehydrogenase (LDH) assay and cells were fixed with 4% paraformaldehyde for 15 min. After the fixation step the samples were washed 3 times with PBS and permeabilized with PBS + 0.1% triton for 15 min. Then, they were blocked with PBS + BSA (0.3%) for 15 min and finally anti-H2AX monoclonal antibody (Abcam Cambridge, United Kingdom) was added at 1/500 in PBS + 0.3% BSA for 60 min at room temperature. After three washing steps, the secondary goat anti-mouse antibody Alexa 633 (Invitrogen) was added at 1/500 for 60 min to react against the primary antibody. The samples were then washed three times and measured in the Pathway 855 automated fluorescent microscope. H2AX fluorescence intensity was detected in the nucleus.

#### 2.4.4. LDH assay

The LDH assay was performed according to the manufacturer's protocol. Fully automated cytotoxicity detection kit (LDH)(Roche, Mannheim, FR, Germany) was used to measure LDH release in milliunits per liter (mU/L) in culture media obtained from breast cancer cell line

subjected to antioxidant treatments described above for 24 h. The release of LDH from cells with damage plasma membrane into the culture medium was assayed by incubating the clarified culture medium with sodium pyruvate in the presence of NADH. Pyruvic acid is catalyzed into lactic acid by free LDH along with a simultaneous oxidation of NADH to NAD+. The rate of oxidation of NADH to NAD+ was measured at 340 nm using Synergy 2 Multi Mode Microplater reader Biotek (Winooski, USA).

*2.4.5. Mitotic arrest*

Mitotic arrest staining was determined by immunohistochemistry (IHC). Cells were fixed directly with 16% paraformaldehyde for a final concentration of 4% for 15 min. After the fixation step the samples were washed three times with PBS and permeabilized with PBS + 0.1% triton for 15 min. The samples were then blocked with PBS + BSA (0.3%) for 15 min and finally anti-phospho-H3 polyclonal antibodies (Invitrogen) were added at 1/500 in PBS + 0.3% BSA for 60 min a room temperature. After three washing steps, 4′,6-diamidino-2-phenylindole (DAPI) and the secondary antibodies Alexa 488 (Invitrogen) were added at 1/500 for 60 min to react against the primary antibody. The samples were then washed three times and measured in the Pathway 855 automated fluorescent microscope. This antibody allows the direct quantification of mitotic cells.

At least three independent experiments were performed for each experimental condition in all the biological assays. The results are expressed as the mean ± standard error of the mean.

*2.5. Fluorescence quenching measurements*

BSA was dissolved in Tris–HCl (0.1 M, pH 7.4) buffer to attain a final concentration of 6 μM. Naringenin, oxidovanadium(IV) cation and VOnar, were added dropwise to the BSA solution and left to rest to ensure the formation of homogeneous solutions with concentrations ranging from 2 to 100 μM. The fluorescence intensity was measured (excitation at 280 nm and emission at 348 nm) at 25 °C. For each sample and concentration, three independent replicates were performed. The measurements were carried out on a Perkin-Elmer LS-50B luminescence spectrometer (Beaconsfield,England) equipped with a pulsed xenon lamp (half peak height < 10 ls, 60 Hz), an R928 photomultiplier tube and a computer working with FLWinLab software. Both excitation and emission slits were set at 10 nm throughout this study.

## 3. Results and discussion

*3.1. FTIR spectroscopy*

The FTIR spectrum of VOnar has been compared to that of naringenin to validate the proposed structure of the complex. Typical spectral band shifts for the new compound matches those previously determined and assigned for other VOflavonoids [10–14], and in particular are comparable to those of VOchrysin that encloses a similar structure (except the presence of both the C2=C3 double bond (chrysin) and the 4′-OH group (nar)). The characteristic C=O stretching band of naringenin shifts from 1634 $cm^{-1}$ to 1614 $cm^{-1}$ upon coordination, showing its interaction with the metal center. The band associated with the vibrational deformation modes of the 5-OH and 7-OH groups (1601 $cm^{-1}$) of naringenin appears as a shoulder of low intensity in the complex. These results suggest that the V=O cation coordinates through the carbonyl oxygen and the 5-$O^-$ group (ring A). This chelate formation is responsible for the increase in the C=O bond length with the concomitant shift of the position of the band of its stretching mode in 20 $cm^{-1}$ to low wavenumbers. The new bands located at 1540 $cm^{-1}$ and 1441 $cm^{-1}$ have been assigned to the antisymmetric and symmetric C5–O5 stretching modes at the chelating site. The band of the C–O–C stretching mode (ring C) at 1251 $cm^{-1}$ is not modified by metal coordination, indicating the absence of interaction of this group with the metal center. The broad band at 973 $cm^{-1}$ that appeared overlapped with the band of the ligand at 968 $cm^{-1}$, has been assigned to the characteristic V= O stretching mode. The position of the $\nu$(V=O) band is typical for the oxidovanadium(IV) ion coordinated to the C=O and OH groups of flavonoids in a chelated form (Fig. 2A).

*3.2. Electron paramagnetic resonance (EPR) and magnetic data*

The X-EPR powder spectrum of the complex was recorded at room temperature (Fig. 3A). The observed signal is a broad and quasi-isotropic line with g = 1.97 typical to vanadium (IV) complexes. A computer simulation provides the following spin Hamiltonian parameters: $g_{//} = 1.968$ and $g_{\perp} = 1.976$ ($g_{iso} = 1.973$), reflecting small anisotropy in good agreement with a oxidovanadium(IV) ion in a nearly axial or pseudoaxial ligand field. The absence of the hyperfine structure expected for isolated $V(IV)O^{2+}$ chromophores (100% abundant $^{51}V$ nucleus) suggest a polynuclear arrangement, being the observed spectrum the result of the mutual interactions between neighboring $V(IV)O^{2+}$ sites [11]. It should be noted that the EPR line corresponds to a collective resonance when the exchange interaction (J) between magnetic ions in different lattice sites is larger than the difference between their Zeeman energies.

For this reason, magnetic susceptibility measurements of VOnar between 5 and 300 K have been performed. The thermal variation of the inverse of the magnetic molar susceptibility ($\chi_m^{-1}$) and the $\chi_m T$ product is shown in Fig. 3B. Over the entire temperature range, the magnetic susceptibility follows a Curie–Weiss law with $C_m = 0.37$ $cm^{3-}$ K $mol^{-1}$ and $\theta = +2.1$ K. The observed Curie constant agrees quite well with the calculation from the g value (0.36 $cm^3$ K $mol^{-1}$). The magnetic effective moment continuously increases on cooling, more quickly below 20 K. Both, the positive temperature intercept and the increase of the magnetic effective moment at low temperatures are in agreement with the slight ferromagnetic interactions in the compound.

Due to lack of crystallographic data, different models were used to adjust the observed magnetic behavior and determine the nature of the polynuclear arrangement: dimers, chains or layers. Finally, experimental data could only be satisfactorily fitted using the analytical expression, Eq. (1), that describes the behavior of a regular chain with S = 1/2 using an isotropic Heisenberg Hamiltonian $\mathbf{H} = -2J\Sigma S_i S_{i+1}$ [16]

$$\chi_m = \frac{Ng^2\beta^2}{4kT}\left(\frac{1 + A_1x + A_2x^2 + A_3x^3 + A_4x^4 + A_5x^5}{1 + B_1x + B_2x^2 + B_3x^3 + B_4x^4}\right)^{2/3} \quad (1)$$

$$x = J/k\,;\ A_1 = 5.798\,;\ A_2 = 16.902\,;\ A_3 = 29.377\,;\ A_4 = 29.833\,;$$
$$A_5 = 14.037\,;\ B_1 = 2.798\,;\ B_2 = 7.009\,;\ B_3 = 8.654\,;\ B_4 = 4.574$$

where N and k are the Avogadro and Boltzmann constants, respectively, and β is the Bohr magneton. The best fit was obtained by minimizing the reliability R factor, $R = \Sigma[\chi_m T^{exp} - \chi_m T^{cal}]^2/\Sigma[\chi_m T^{exp}]^2$. As can be observed in Fig. 3C, an excellent agreement between theoretical and experimental data could be obtained with g = 1.98 and J/k = +0.6 K ($R = 1.5 \times 10^{-5}$). Therefore, the observed ferromagnetic behavior in this compound corresponds to the interactions propagated along regular chains of $V(IV)O^{2+}$ ions (Fig. 2B). This result is also concordant with the no observation of the "half-field" signal on the EPR spectra and confirms the absence of dimeric entities in the system.

*3.3. Solution studies*

Naringenin exhibits two major absorption bands in the UV–vis region and their position and intensity strongly depend on the pH value of the solution. The absorption band in 290–330 nm range corresponds to the B ring portion (cinnamoyl system, band I), and the absorption band in 225–250 nm range corresponds to the A ring portion (benzoyl system, band II) (Fig. 4A). The flavanone has a saturated

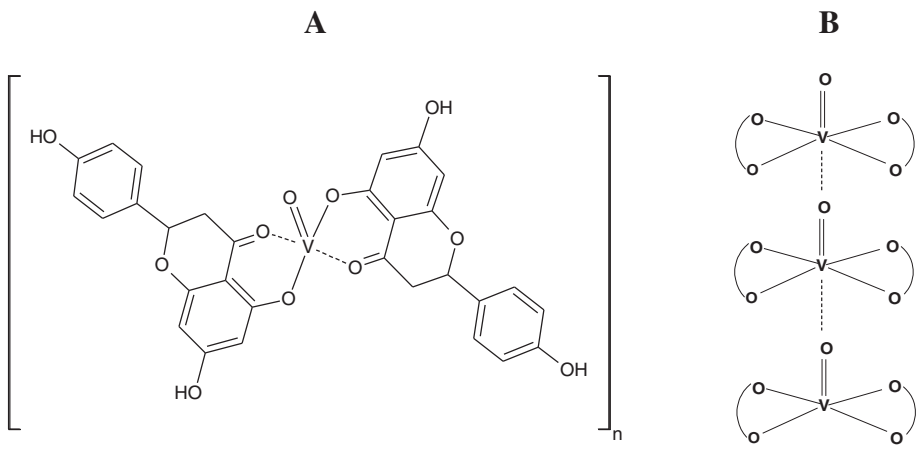


**Fig. 2.** Schematic representation of the structure of the $[V^{IV}O(nar)_2]\cdot 2H_2O$ complex (A) and the chains O=V–O=V– proposed from magnetic determinations (B).

heterocyclic ring C (Fig. 1) with lack of conjugation between the A and B rings and a concomitant stronger separation of the HOMO and LUMO orbitals on the B and A rings. This absence of conjugation leads to a shift of the main absorption band to the blue in relation to other flavonoids [17,18].

The protonation constants of naringenin in aqueous solution at 25 °C were found to be: $pK_1 = 6.7$, $pK_2 = 9.1$; $pK_3 = 13.0$. By spectral analysis it was demonstrated that $pK_2$ corresponds to ionization of 4′-OH (ring B), $pK_1$ to 5-OH and $pK_3$ to 7-OH, both in the A ring of the molecule [19]. The electronic spectral pattern of naringenin in ethanolic solution depends strongly on the pH of the solution. The band at 250 nm increases in intensity at pH values higher than 10 and is an indication of the third deprotonation of naringenin at ring A (7-OH). The band at 290 nm decreases between pH 8–10 and that at 330 nm increases in intensity at the same pH range and exhibits an isosbestic point, which is indicative of the presence of equilibrium between the two forms of naringenin ($narH_2^-$ and $narH^{2-}$). This shift is in accordance with an electronic change in ring B, pointing to the ionization of the 4′-OH group ($pK_2 = 9.1$). To measure the pKa values the change in the absorbance at 330 nm is plotted against the pH (Fig. 4B). A nonlinear regression allowed the determination of $pK_2$ (9.2), comparable with earlier reported data [20] The $pK_3$ value cannot be obtained by a direct determination. From the plot of the absorbance at 250 nm *vs.* pH the curve suggests that the third deprotonation will occur with a $pK_3$ near 13, similar to the reported data (not shown).

After the interaction with oxidovanadium(IV) ion, no appreciable changes were observed in the UV–vis spectra at different pH values. The coordination of the metal has been determined to be due to the formation of a new six-membered ring system between the metal ion and the oxygen atoms from 4-oxo and 5-OH sites (see above), and may affect the transitions on ring A (225 nm). The shift of this band to lower energies seems to be equivalent to that of naringenin and occurs at pH values higher than 10, like naringenin. The absence of C2–C3 double bond in the flavonoid makes the rings not planar without conjugation between rings B and C. Then, the same pattern found for the variation of Band I with pH for naringenin and VOnar (see Fig. 5), is indicative of the lack of interaction of the cinnamoyl moiety with the metal center. The stoichiometry of the new complex was determined by the molar ratio method at 290 nm Fig. 6. A L:M 2:1 ratio has been obtained from Fig. 6, inset.

The electronic spectra of VOnar in the visible range (working with 2:1 L:M ratios, 0.015 M VOnar) support that the coordination of the metal to the ligand takes place. In Fig. 7A it can be seen that the typical spectrum of $[V^{iV}O(H_2O)_5]^{2+}$ is observed at pH values lower than 3. At higher pH values, the band of the oxidovanadium(IV) at 620 nm (Band 2, $3d_{xy} \rightarrow 3d^2_{x-y^2}$) shifted to 576 nm (pH 3.5–8, in absolute ethanol). To a better assignment, deconvolution of the band in the 800–350 region was performed (Fig. 7B). It can be seen that the band of the oxidovanadium(IV) cation at 760 nm (Band 1, $3d_{xy} \rightarrow 3d_{xz,yz}$) appeared at 673 nm and 762 nm. This shift agrees with the presence of environments with oxygenated coordination spheres around the metal center similar to other "acetylacetone-like" or "maltol-like" coordination systems [21] of the oxovanadium(IV) complexes of chrysin, silibinin, morin and quercetin [3,14]. At pH values higher than 8 hydrolytic processes took place with the possible formation of hydroxo vanadium complexes like $(VO)_2(OH)_5^-$ and $VO(OH)_3^-$. No precipitation of $VO^{2+}$ hydrolytic products was observed during the experience.

The diffuse reflectance spectra of VOnar showed the band 2 at the same position *ca.* 570 nm. The pattern of band 1 (higher than 800 nm $d_{xy} \rightarrow (d_{xz}, d_{yz})$) is in accord with those VOflavonoids of silibinin and morin previously reported [13,14]. The shift of this band to the blue upon dissolution may be due to the rupture of the polymeric structure and the consequent solvation effects that increase the crystal field splitting of the orbitals lying in the x,z and y,z planes.

The stability of the complex in ethanolic solution was followed by UV–vis spectroscopy and it was found that in 60 min there were no spectral changes (data not shown), indicating that during the manipulation time for biological studies (15 min) the complex remained stable and without decomposition.

As the EPR technique is a more sensitive method for the detection of vanadium species in solution than the electronic spectra, the EPR spectrum (X-band) has also been measured from the dissolution of the solid complex in DMSO (140 K, 20 mM) to determine whether the structure of the solid complex has been retained in solution Fig. 8A. The solvent used for biological measurements, DMSO, has been selected for this measurement. The EPR signal shows the typical eight-line-pattern spectrum for $V^{IV}O$ systems. This signal indicated the formation of single mononuclear species after the dissolution process. The spectral simulation (Fig. 8B) predicted the formation of a $V^{IV}O$ chromophore with spin Hamiltonian parameters $g_z = 1.944$, $g_x = 1.978$, and $g_y = 1.982$ and hyperfine coupling constants of $A_z = 169 \times 10^{-4}\ cm^{-1}$, $A_x = 62 \times 10^{-4}\ cm^{-1}$, and $A_y = 59 \times 10^{-4}\ cm^{-1}$ ($g_{iso} = 1.968$, $A_{iso} = 96.67 \times 10^{-4}\ cm^{-1}$). From the EPR parameters it has been estimated that the conformation of the solution complex would most probably correspond to a binding mode of 2(CO, $O^-$) possibly including a solvent molecule (DMSO) in the sixth position of the coordination sphere. Using the additivity rule, this assumption gives a calculated value of $Az = 166.6 \times 10^{-4}\ cm^{-1}$ (C=O

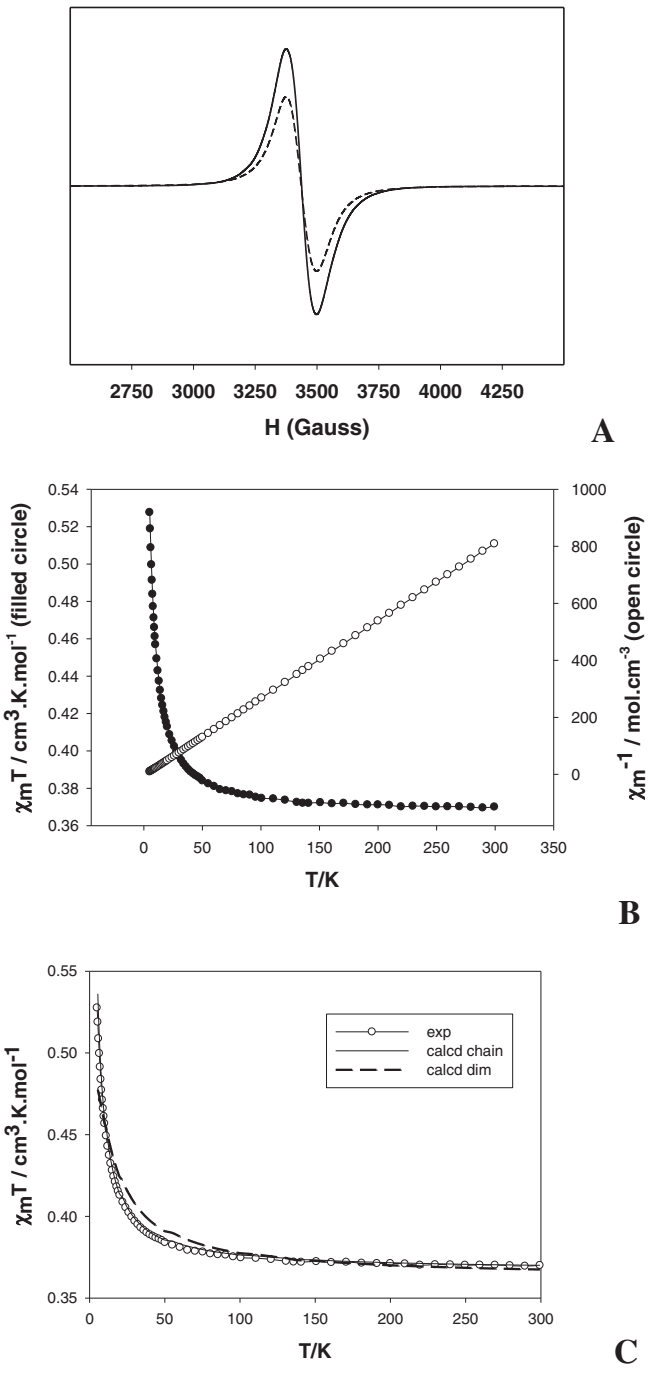


**Fig. 3.** A) Experimental (—) and calculated (– – –) room-temperature powder electron paramagnetic resonance spectrum of the $[V^{IV}O(nar)_2]\cdot 2H_2O$ complex (VOnar) measured at X-band, 298 K. B) Temperature dependence of the magnetic susceptibility and the $\chi_m T$ product of VOnar. C) Fit of the magnetic data.

$44.7 \times 10^{-4}$ cm$^{-1}$, ArO$^-$ $38.6 \times 10^{-4}$ cm$^{-1}$) in good agreement with the values reported for "acetylacetone-like" coordination assuming trans configuration (V=O/solvent) in solution [12,21].

### 3.4. Antioxidant activities

According to the structure–activity relationship it can be seen that the absence of the hydroxyl group at position 3 in flavanones and flavones renders a decrease in their antioxidant ability and also does the absence of the catechol structure in the B-ring [22]. However, taking into account that the flavonoids have the ability to capture electrons on the hydroxyl groups, the presence of a C2=C3 double bond also confers great stability when the radical is formed, then preventing the

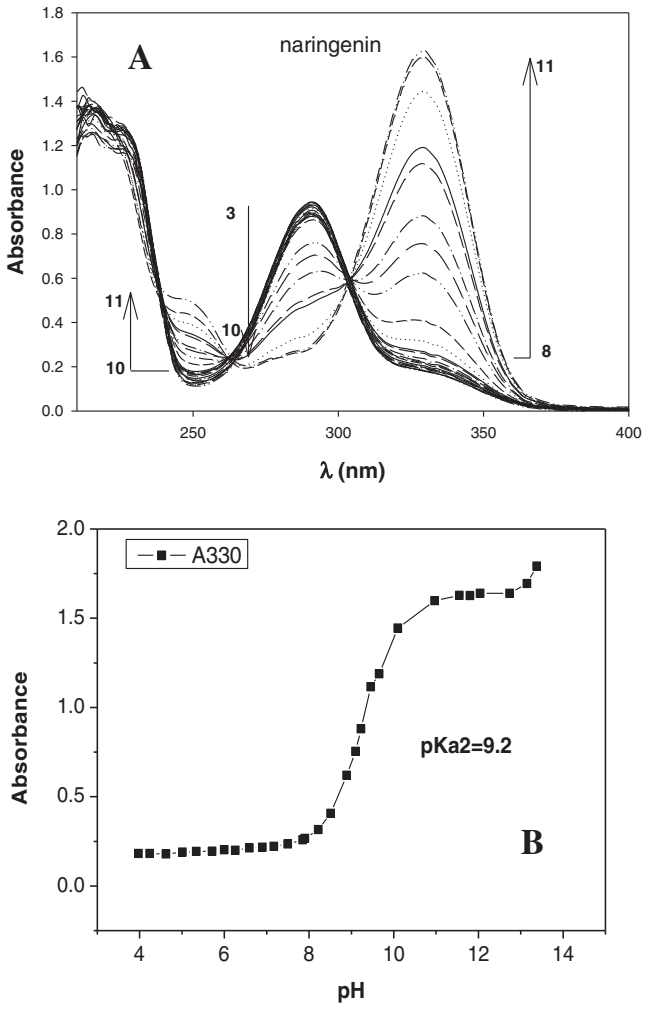


**Fig. 4.** A) Electronic spectral data of ethanolic solutions of naringenin ($4 \times 10^{-5}$ M) with pH adjusted by minimal addition of 1 M NaOH and 1 M HCl. B) Effect of pH on the absorbance of naringenin ($\lambda = 330$ nm); pKa determination.

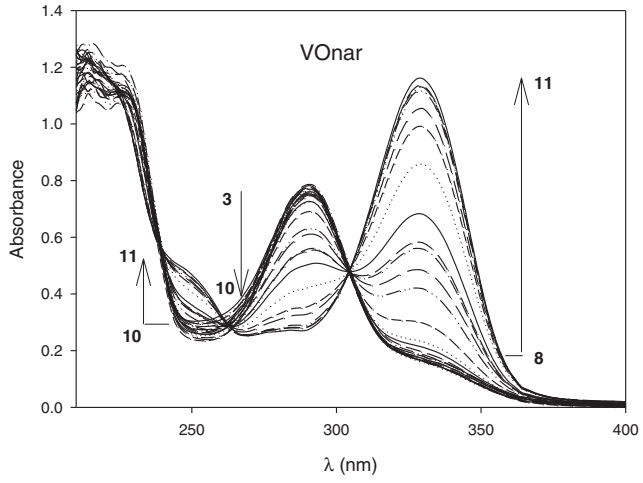


**Fig. 5.** Electronic spectral data of ethanolic solutions of naringenin ($4 \times 10^{-5}$ M) and $VOCl_2\cdot 2H_2O$ ($2 \times 10^{-5}$ M). The pH values were adjusted by minimal addition of 1 M NaOH and 1 M HCl form 3 to 11.

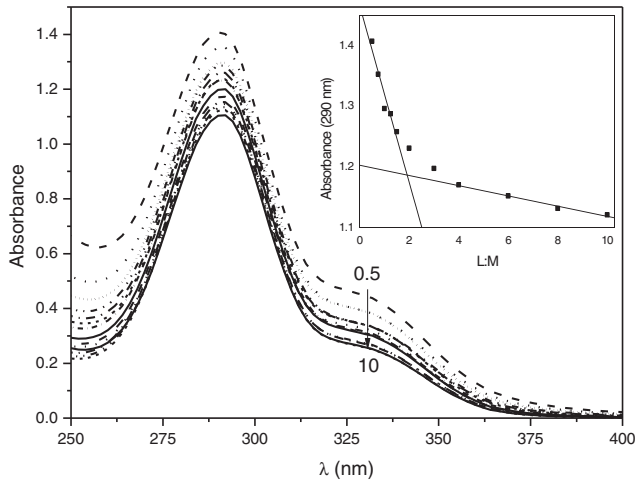


**Fig. 6.** Electronic spectra of ethanolic solutions of naringenin ($5 \times 10^{-5}$ M) with the addition of $VOCl_2 \cdot 2H_2O$ in ligand-to-metal ratios (L/M) from 10 to 0.5. The pH was adjusted to 8 with an ethanolic solution of 5% of $NH_3$. Inset: spectrophotometric determination of the VOnar complex stoichiometry at 290 nm by the molar ratio method.

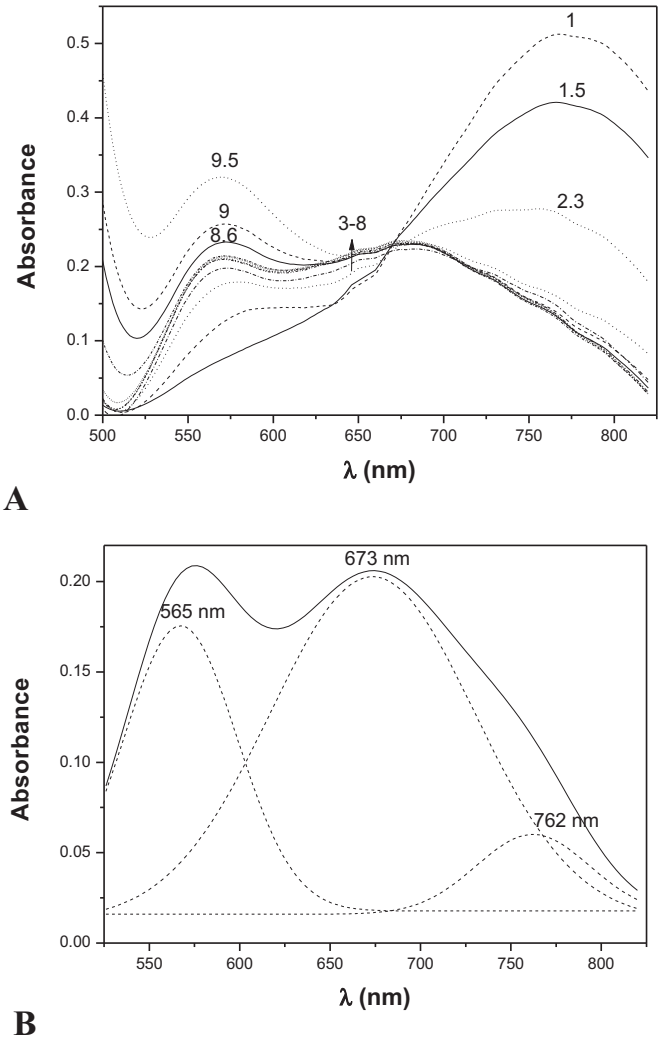


**Fig. 7.** Electronic absorption spectra of $VOCl_2 \cdot 2H_2O$ ($1.5 \times 10^{-2}$ M) and naringenin ($3 \times 10^{-2}$ M) in ethanolic solutions, for different pH values, adjusted with 1.5 M $NH_3$ and 1 M HCl (A). Deconvolution of the spectrum at pH 8 (B).

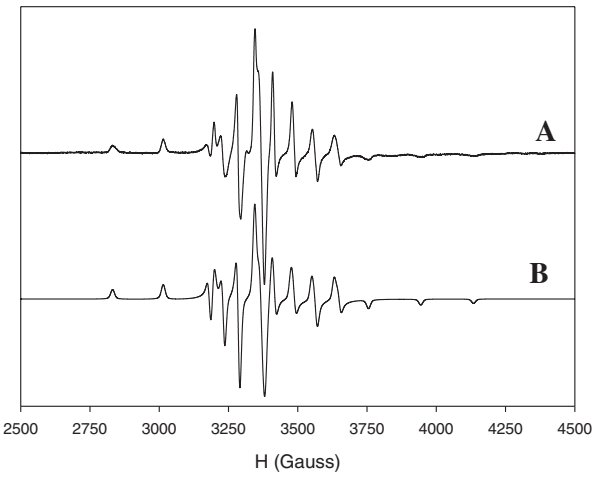


**Fig. 8.** EPR of a DMSO solution spectrum (20 mM, 140 K, X-band) of $[VO(nar)_2] \cdot 2H_2O$ (A) and computer simulation (B, WINEPR SimFonia).

propagation of chain reactions of the oxygen free radicals [23]. For this reason it is expected that naringenin without the 3-OH and the double bond at C2–C3 positions in its structure may have low antioxidant activities. In fact, the percentage of DPPH• scavenging power at 100 μM was very low (4 ± 2) (Table 1). When antioxidants interact with DPPH• they transfer one electron or hydrogen atom and thus neutralize its free-radical character. The very weak capacity for naringenin to scavenge DPPH• radical has also been explained as owing to the absence of O-dihydroxy group on ring B [24–26].

The capacity of suppressing the radical cation ABTS•$^+$ was determined by the TEAC assay considering a value of 1 for Trolox. An experimental value of 2.4 has been obtained for naringenin, corresponding to near the half of that of one of the best antioxidant among flavonoids, quercetin. However, different TEAC values ranging from 1.14 to 2.69 [25,27–29] have been reported for naringenin illustrating the significance of the absence of the saturation of C2–C3 bond. Previous data showed that for the TEAC assay the activity of naringenin was almost zero, displaying low to no antioxidant activity in the TEAC [26,30,31].

The SOD activity had been defined as the concentration of the tested compounds that produce the 50% inhibition of the NBT reduction by the superoxide anion produced in the system ($IC_{50}$ value). The superoxide reduction power for naringenin was found to be higher than 100 μM (namely, with no biological effect) like other published data [4,30,32–34].

**Table 1**
Percentage of free radical scavenging power of $V(IV)O^{2+}$ cation, the flavonoids naringenin, quercetin, silibinin, chrysin and morin and their oxidovanadium(IV) metal complexes. Values are expressed as the mean ± standard error of at least three separate experiments.

| Compound | DPPH•[a] | TEAC[b] | $O_2^{-}$[c] | OH•[a] | ROO• |
|---|---|---|---|---|---|
| $V(IV)O^{2+}$ | 37 ± 2 | 0.2 | 15 | 38 ± 2 | 6.4[d] |
| Naringenin | 4 ± 2 | 2.4 | >100 | 50 ± 5 | – |
| VOnar | 67 ± 11 | 4.7 | >100 | 37 ± 2 | 2.9[d] |
| Quercetin | 98[39] | 4.7[40] | 1.6[41] | ** | 26.1[38] |
| VOquer | ND | ND | ND | ND | ND |
| Silibinin | 16 ± 1 | 1.8 | 2.7 | 24 ± 3 | 5.0[e] |
| VOsil | 83 ± 1 | 1.8 | 0.3 | 45 ± 2 | 11.9[e] |
| Chrysin | 18 ± 1 | 0.9 | * | 50 ± 3 | ND |
| VOchrys | 45 ± 2 | 4.0 | 159 | 75 ± 3 | ND |
| Morin | 88 ± 1 | 2.1 | 66 | 30 ± 1 | 5.2[f] |
| VOmor | 90 ± 2 | 2.0 | 54 | 60 ± 3 | 1.8[f] |
| $SOD_{native}$ | | | 0.21 | | |

[a]Percentage of the scavenging power at 100 μM; [b]Trolox equivalent antioxidant capacity; [c]SOD simil activity ($IC_{50}$ (μM)); [d]lag phase (min) at 100 μM, [e]relative ORAC, [f]lag phase (min) at 10 μM, *no activity, ND no determined, **very scattered bibliographic data.

Peroxyl radicals were assayed upon their generation by the thermal decomposition of AAPH (2,2-azobis(2-amidinopropane) dihydrochloride) [35]. The delay of the consumption of the spectrometric probe, pyranine, (lag phase) was calculated as the time due to the consumption of peroxyl radicals by the added compounds, before the consumption of pyranine started [36]. As a result, the lag phase can be used to determine the capacity of a substance to scavenge peroxyl radicals. No activity was found for naringenin against peroxyl radicals. A moderate behavior has been published for the scavenging power of OH• radicals by naringenin [34,37] in agreement with our measurements (50% at 100 μM).

The antioxidant capacities of the flavonoid have been improved by complexation with the oxidovanadium(IV) cation (see Table 1), except for scavenging of the hydroxyl radical. The capacity to scavenge DPPH• radical raised in proportion from 4 to 67% (100 μM). The TEAC value, obtained from the ratio of the slopes relative to trolox, displayed twice the value of the ligand and similar to the quercetin value. The complex also exhibited activity against the peroxyl radicals. An increase in the induction time (lag phase) of the reaction has been observed in a dose response manner. The slope of the straight line obtained in this assay showed that VOnar is more effective in scavenging peroxyl radicals than trolox but is less effective than the oxidovanadium(IV) cation and much less than the flavonoid quercetin [38]. Both the ligand and the complex showed a very low SOD enhancement activity. The $IC_{50}$ value in both cases could not be determined due to the low solubility of both compounds at concentrations higher than 100 μM. The capacity to scavenge OH• radicals upon complexation was slightly lower (37%, 100 μM). However, both compounds behaved as moderate OH• radical scavengers. The antioxidant capacities of related flavonoids and their oxidovanadium(IV) complexes are shown in Table 1 for the sake of comparison [39–41].

### 3.5. Biological assays

#### 3.5.1. In vitro cell cytotoxicity

For the evaluation of cytotoxicity, three different cancer cell lines were used: A549 (lung cancer cell line) and SKBr3 and MDAMB231 (breast cancer cell lines). The effects of the naringenin, VOnar and $V(IV)O^{2+}$ cation were investigated and the half maximal inhibitory concentration (concentration that inhibits 50% cell viability, $IC_{50}$) is shown in Table 2. As discussed earlier, naringenin did not show antitumoral activity against several cell lines (lung A549 adenocarcinoma, colon C26 carcinoma, B16 melanoma, Lewis lung carcinoma (LLC), cervix Hela adenocarcinoma, HT-1080 fibrosarcoma, among others). Several reports have assigned this significantly low activity to the presence of the 5-hydroxyl group in the phenyl ring A on flavanones, [42] or to the lack of the o-catechol moiety in the B ring [43]. Upon substitution of the OH group at C-7 the apoptosis-inducing activity of naringenin derivatives has been improved, demonstrating the notion of the structurally related activities of flavonoids in apoptosis [44]. We have determined herein that the free ligand does not have any cytotoxic effect on the A549 cell viability at 100 μM and that $V(IV)O^{2+}$ cation inhibited only 16% cell viability at the same concentration (data not shown). In opposition, VOnar significantly decreased the viability of lung cancer cells in a dose response manner (35% at 100 μM, data not shown) indicating that the complexation of the flavonoid improved its potential pharmacological properties, though the $IC_{50}$ values for the three compounds resulted higher than 100 μM.

Naringenin behaved as a non cytotoxic agent against SKBr3 breast cancer cells and acted as a more deleterious agent (30% cell viability inhibition at 100 μM, data not shown) against MDAMB231 breast cancer cell lines. It has previously been demonstrated that the presence of the C2–C3 double bond is an important feature for inducing cytotoxicity on different cancer cells and for other pharmacological activities [45]. Other studies showed that naringenin behaved as non-cytotoxic in tested breast cancer cell lines with a high value of $IC_{50}$ (>100 μM) probably due to the lack of the C2 = C3 bond [46–49]. It can then be seen that the structure of the different flavonoids plays a key role in the biological activity of them. We have reported the behavior of flavonoids with better antioxidant properties: quercetin, chrysin, silibinin and morin [10] and found a deleterious effect on the breast cancer cell lines in accordance with their antioxidant activities (see Table 2), hence confirming the relationship between the structure and the activity of the flavonoids. On the other hand, the complex VOnar acted as a high potent agent against both cell lines with $IC_{50}$ values of 73 μM and 20 μM for the SKBr3 and MDAMB231 lines, respectively (Table 2). It can then be assumed that the improvement of the cytotoxic effect by complexation resulted higher in flavonoids with low antioxidant power. In addition, the reported activity of $V(IV)O^{2+}$ established a less antitumoral potency ($IC_{50}$ 96 μM [13] and 49 μM [10] for SKBr3 and MDAMB231, respectively). The metal complexation of the flavonoid enhanced the deleterious effect on the viability of the cancer cell lines probably due to the extended planar structure induced by the p–π* conjugation resulting from the six membered chelate ring formation. This planar structure could induce mechanistic changes such as the damage of DNA [50].

Having identified from the first screening that VOnar inhibitory effects were selective for the breast cancer cell lines, their mechanism of action was investigated in the SKBr3 and MDAMB231 cells. Cells were treated with VOnar (at the $IC_{50}$ concentrations, 24 h incubation) and with the specific concentration of naringenin and $V(IV)O^{2+}$ contained in those concentrations, to obtain toxicity without affecting a reasonable number of viable cells. To confirm the possible cell death pathway we have investigated the effects of the compounds on intracellular ROS production, mitochondrial membrane potential disruption, caspases 3/7 activation, induction of LDH release, nuclear damage (H2AX), mitotic arrest and intracellular glutathione (Table 3).

**Table 2**
Half maximal inhibitory concentration (concentration that inhibits 50% cell viability, $IC_{50}$) of oxovanadium(IV) cation ($V(IV)O^{2+}$), naringenin, and the complex VOnar in breast cancer cells. Cells were incubated in basal medium alone or with increasing concentrations of the compounds at 37 °C for 24 h. The $IC_{50}$ calculation was performed using Sigma plot 10.2.2 software. Comparison with the antitumoral effects of the flavonoids quercetin, silibinin, chrysin and morin and their oxidovanadium(IV) metal complexes (Taken from Refs. [10] and [14] ND: not determined.

| | Cell lines/$IC_{50}$ values (μM) | |
|---|---|---|
| | SKBr3 | MDAMB231 |
| $V(IV)O^{2+}$ | 96 | 49 |
| Naringenin | >100 | >100 |
| VOnar | 73 | 20 |
| Quercetin | 26 | 50 |
| VOquer | 23 | 10 |
| Silibinin | 36 | 21 |
| VOsil | 5 | 6 |
| Chrysin | >100 | 58 |
| VOchrys | 6 | 3 |
| Morin | 86 | ND |
| VOmor | 63 | ND |

#### 3.5.2. Intracellular ROS generation

It is a well-known fact that many types of cancer cells have elevated levels of ROS compared with their normal counterparts [51]. Oxidative stress due to increase in the level of intracellular ROS leads to a variety of biochemical and physiological lesions followed by metabolic impairments and cell death. The stimulus of free radicals and oxidative stress can trigger the mitochondrial initiated events leading to the activation of the intrinsic pathway. Several reports have shown that a host of phenolic phytochemicals, including flavonoids, can alter intracellular ROS levels [44]. To investigate this association, the levels of intracellular ROS were determined by DCFH-DA assay. This probe recognizes several intracellular oxidant species and other peroxides [52]. Results obtained demonstrated that SKBr3 and MDAMB231 cells treated with VOnar

**Table 3**
High Content cytotoxicity assay Effect of naringenin, oxovanadium(IV) cation ($V(IV)O^{2+}$) and the complex in the MDAMB231 and SKBr3 cell lines, for ROS production, disruption of the mitochondrial membrane potential (TMRM), Caspase 3/7 activation, damage of the plasmatic membrane (LDH) measurements, DNA-damage (histone phosphorylation, H2AX) and mitotic arrest. Results are expressed as percentage of the measured basal level and represent the mean values ± the standard error of the mean (SEM) from three separate experiments.

| | MDAMB231 | | | SKBr3 | | |
|---|---|---|---|---|---|---|
| Compound | VOnar | Naringenin | $V(IV)O^{2+}$ | VOnar | Naringenin | $V(IV)O^{2+}$ |
| ROS | 157 ± 2.3* | 100 ± 2.3 | 98 ± 2.4 | 153 ± 20* | 97 ± 6.5 | 101 ± 7.9 |
| TMRM | 76 ± 5.5* | 100 ± 1.4 | 109 ± 5.5 | 84 ± 2.2 | 99 ± 2.1 | 96 ± 3.5 |
| CASPASE 3/7 activation | 597 ± 35* | 105 ± 33 | 115 ± 17 | 176 ± 21* | 98 ± 35 | 101 ± 0 |
| LDH | 305 ± 40* | 134 ± 10* | 139 ± 8.3* | 248 ± 49* | 123 ± 8.7* | 105 ± 3.8 |
| H2AX | 155 ± 19* | 114 ± 34 | 141 ± 9.0 | 137 ± 11* | 96 ± 7.0 | 94 ± 6.0 |
| Mitotic arrest | 127 ± 21* | 102 ± 17 | 68 ± 8.0 | 198 ± 21* | 96 ± 5.0 | 51 ± 8.2 |

Basal values: 100%; *toxicity: higher than ±20% from basal.

showed similar and significant production of oxidizing species (1.5 fold higher) when compared to the basal rate Fig. 9A. However, no ROS production was observed for naringenin and for the oxidovanadium(IV) cation treated cells. Among ROS, the oxovanadium(IV) cation behaves as a better scavenger of superoxide anions and peroxyl radicals (see Table 1) and naringenin is a better scavenger of hydroxyl radicals than VOnar. This may be one of the reasons of the cellular enhancement of ROS production observed for the complex. Thus it has been determined that metal complexation of the flavonoid enhanced ROS production in both breast cancer cell lines.

### 3.5.3. Mitochondrial damage

To better characterize the apoptotic death triggered by VOnar, the role of mitochondria was investigated. The decrease of mitochondrial membrane potential ($\Delta\Psi m$) causes the disruption of the outer mitochondrial membrane and contributes to the release of cytochrome c. Therefore, the cytochrome c release results in the activation of caspase-9 and subsequently leads to apoptosis [53]. The evaluation of mitochondrial membrane potential was performed using TMRM dye. The results revealed polarized normal cells in control cells and naringenin and $V(IV)O^{2+}$-treated cells whereas VOnar treatment showed population of depolarized cells after 24 h of exposure in both cell cultures but differences in SKBr3 cells were not >20%. Fig. 9B. The most sensitive effects of VOnar were observed at 6 h of treatment in which decreases of 60% and 40% were observed in MDAMB231 and SKBr3 cells, respectively (data not shown). Thus, it can be concluded that the metal complexation of the flavonoid decreased mitochondrial membrane potential mainly in MDAMB231 cancer cell line.

### 3.5.4. Apoptosis activation

Two major groups of caspases have been identified to be involved in apoptosis pathways, including effectors (caspase-3, -6, -7) and initiators

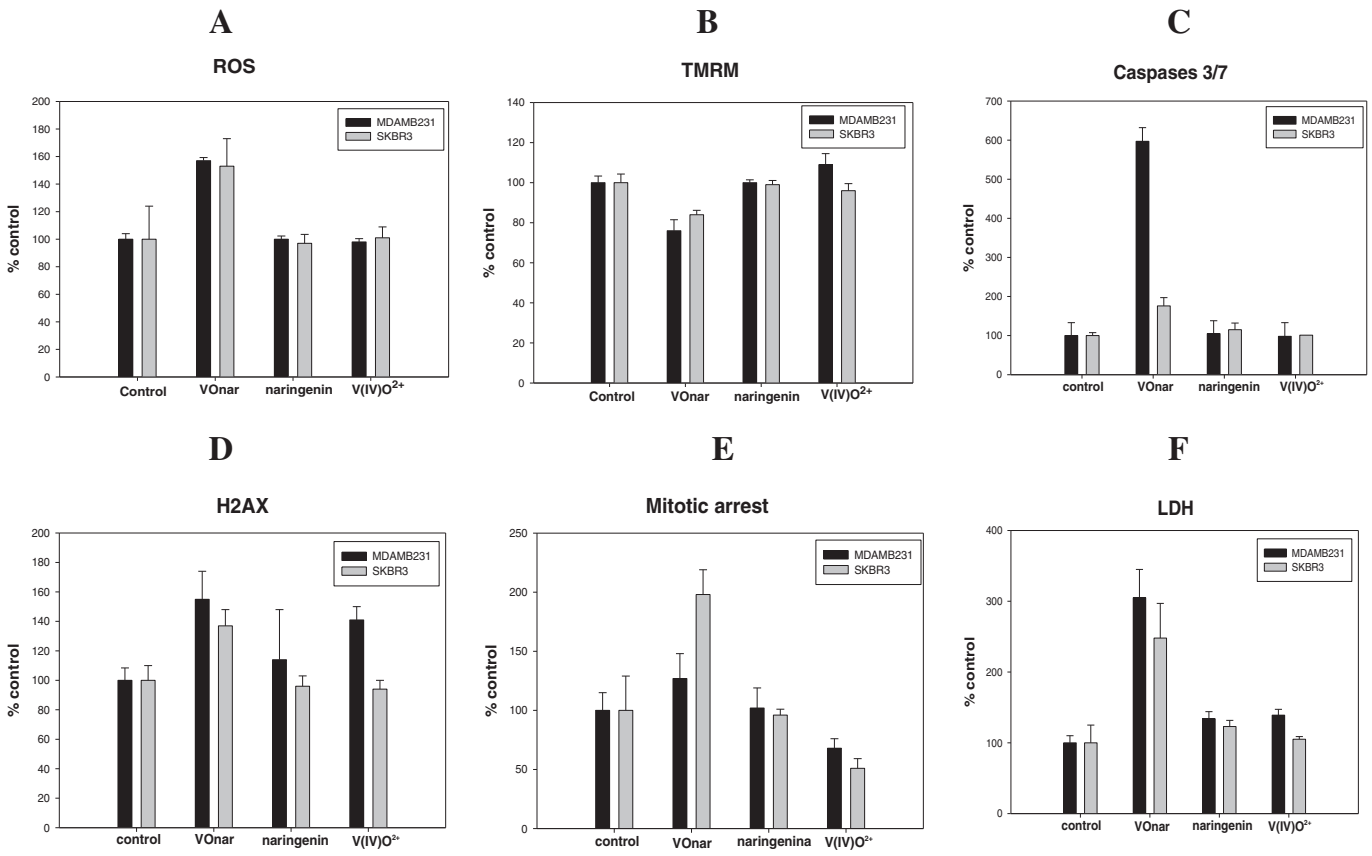


**Fig. 9.** Results for the MDA-MB231 (black) and SKBr3 cell lines (gray) incubated with naringenin, the oxovanadium(IV) cation ($V(IV)O^{2+}$) and VOnar at 37 °C at the concentration of the $IC_{50}$ of the complex. A. Reactive oxygen species generation. B. Mitochondrial membrane potential disruption (TMRM). C. Caspase 3/7 activation. D. DNA damage (H2AX). E. Mitotic arrest. F. Plasmatic membrane damage (LDH). Results represent the mean values ± the standard error of the mean (SEM) from three separate experiments.

(caspase -2, -8, 9, 10) [54]. Intrinsic and extrinsic pathways are activated by their own initiator caspases, namely caspases 9 and 8 respectively. The activation of initiator caspases will, in turn, lead to activation of executioner caspases. The most critical of executioner caspases is considered to be caspase 3/7. The execution pathway leads to cytomorphological changes, namely chromatin condensation, cell shrinkage, and formation of apoptotic bodies followed by phagocytosis of the apoptotic cell. In the present study, it was investigated whether VOnar could activate caspase 3/7 in cells treated with the compounds for 24 h. The data in Fig. 9C showed that treatment of VOnar caused an increase of 500% and 76% (respect to basal) for caspase 3/7 activation in MDAMB231 and SKBr3 cells, respectively. However, no caspase activation was observed in naringenin and VO-treated cells. Again, it is interesting to observe that only VOnar induced caspase 3/7 activation and this activation was higher in MDAMB231 cells.

*3.5.5. Nuclear damage*

Previous studies for mammalian cells indicated that the phosphorylation of the subtype of histone H2A, called H2AX, in the position of Ser139 occurs in response to DNA double-strand break (DSB) formation [55]. In other reports it has been determined that flavones with C2 = C3 double bond and planar structure are capable of intercalative binding with DNA. As a consequence, naringenin is then not able to intercalate and damage DNA and this could be due to its non-planar structure (Fig. 9D) [56]. On the contrary, VOnar produced an increase of histone phosphorylation with simultaneous damage of DNA in both breast cancer cell lines (about 1.5 and 1.3 fold higher in MDAMB231 and SKBr3 cells respectively) when compared to the basal rate. Metal complexation of the flavonoid enhanced DNA damage in both cancer cell lines and the effect was higher in MDAMB231 cells. Besides, it can be observed that $V(IV)O^{2+}$ exerted DNA damage in MDAMB231 treated cells but with a lower value than that of the complex.

*3.5.6. Mitotic arrest*

Cancer is often considered as a disease of cell cycle deregulation. Cell size, extracellular growth signals and DNA integrity are tightly regulated by multiple checkpoints in cell cycle progression. Cancer can originate from perturbation in the expression of positive or negative regulators of cell cycle machinery leading to abnormal proliferation of cancer cells. Thus, induction of cell cycle arrest in cancer cells is considered to be one of the crucial cancer treatment strategies. An immunohistochemistry test was performed to evaluate the effect of VOnar on the mitosis-specific antibody anti-phosphohistone H3, PHH3 positive cells and then the mitotic index (pHH3 positive nuclei/all nuclei) was quantified. After 24 h of exposure to the compounds, the percentage of cells with PHH3 positive cells was higher in VOnar-treated cells, and an increase of 27% and 98% was observed in MDAMB231 and SKBr3 cells respectively (Fig. 9E).

*3.5.7. Induction of LDH release*

The stable cytosolic enzyme LDH catalyzes the oxidation of L-lactate to pyruvate and is a measure of the integrity of the cell membrane. Upon membrane damage, LDH enzyme is released into the culture medium, suggesting the loss of membrane integrity and therefore it is applied to detect apoptosis [57]. As a result, to further confirm the cytotoxic effects of compounds on cancer cells, LDH assay was also performed as another indicator of cytotoxicity. As shown in Fig. 9F, a slight LDH increase in naringenin and VO-treated cells was observed. In addition, LDH leakage of MDAMB231 and SKBr3 was significantly increased with the presence of VOnar by 3 and 2.5 fold higher, respectively. Thus, the metal complexation of the flavonoid enhanced again cancer cytotoxicity by increasing LDH release and this activation was higher in the MDAMB231 cell line.

*3.5.8. Intracellular glutathione*

Glutathione (L-glutamyl-L-cysteinyl-glycine, GSH) in cancer cells is relevant in the regulation of carcinogenic mechanisms and its biochemistry deregulation in tumors has been observed in different types of cancers. Cancer cells have higher GSH levels than the surrounding normal cells. Therefore, selective tumor depletion of this peptide presents a promising strategy in cancer treatment. Basal levels of GSH were higher in SKBr3 as compared with MDAMB231 cells (989 ± 15 *vs* 775 ± 24). After 24 h exposure, no compound was able to reduce GSH levels from their basal level in both cancer cell lines (data not shown).

In conclusion, naringenin produced a slight loss of the plasma membrane integrity detected by means of the LDH release. The results of the behavior of naringenin agree with those of S. Yadegarnynia et al. [47]. They have shown that only the cytotoxic flavonoids were able to inhibit mitochondrial outer membrane permeability, and that both cytotoxic and non-cytotoxic flavonoids (like naringenin) can transverse the cell membrane to enter MDAMB231 cells at different levels. This latter effect was found to be greater for the complex. As a result, the higher deleterious effect of the complex could be explained on the basis of the higher interaction with DNA due to the chelation of the metal through the C = O and OH groups generating a six-membered planar structure and electron delocalization on the A ring. Alternatively, the DNA damage could produce a high cellular level of ROS. The anti-proliferative effect of VOnar was accompanied by cell cycle arrest, caspase activation and mitochondrial potential reduction. ROS production and/or GSH depletion induced cellular redox imbalance in cancer cells and as a consequence, cell cycle arrest was observed [58,59]. The decrease of GSH and/or the increase in ROS have been related to mitochondrial disruption, apoptosis activation and DNA damage which is at least responsible for mitotic arrest. Although the mechanism of action of VOnar was similar in both cell lines, the higher parameters observed for the MDAMB231 could be related to the low antioxidant machinery hold by this cell line (low GSH content). Besides, $V(IV)O^{2+}$ cation evidenced DNA and plasmatic membrane damages in the MDAMB231 cell line being these effects negative for the SKBr3 cell line.

*3.6. Binding characteristics of the naringenin and VOnar to BSA*

Plasma albumin is the major drug-binding protein and may act as a drug binding, transporter and delivery. A drug may become bound to plasma proteins to a greater or lesser degree, depending on different factors, such as plasma pH, concentration of plasma proteins, concentration of the drug, and the presence of another agent with a greater affinity for the limited number of binding sites. The degree of plasma–protein binding and the affinity of a drug for the nonspecific protein-binding sites are of great clinical significance. Of equal importance is the readiness with which drugs dissociate from plasma proteins. Those that are more tightly bound tend to have much longer elimination half-lives because they are released gradually from the plasma protein reservoir. To determine the possible interaction and transport of VOnar with albumin, we have investigated herein the binding affinity of bovine serum albumin (BSA) upon its interaction with naringenin and VOnar and compared the values of the ligand and the oxidovanadium(IV) cation with earlier reported data [60].

Fluorescence technique can easily be used as a powerful tool in the study of the interactions, provided that one of the interacting species exhibits an intrinsic fluorescence whose intensity varies when binding to different compounds. When a 6 μM BSA solution is excited at 280 nm, the fluorescence peak occurs at 346 nm (shown in Fig. 10A). This peak is mainly originated by two tryptophan (Trp) residues: Trp-134 and Trp-212. Fig. 10A shows the fluorescence quenching spectra of solutions containing BSA at fixed concentration (6 μM) and different concentrations of each of the studied compounds. It can be appreciated that the addition of increasing concentrations of naringenin and VOnar (Fig. 10B) caused a progressive reduction of the fluorescence

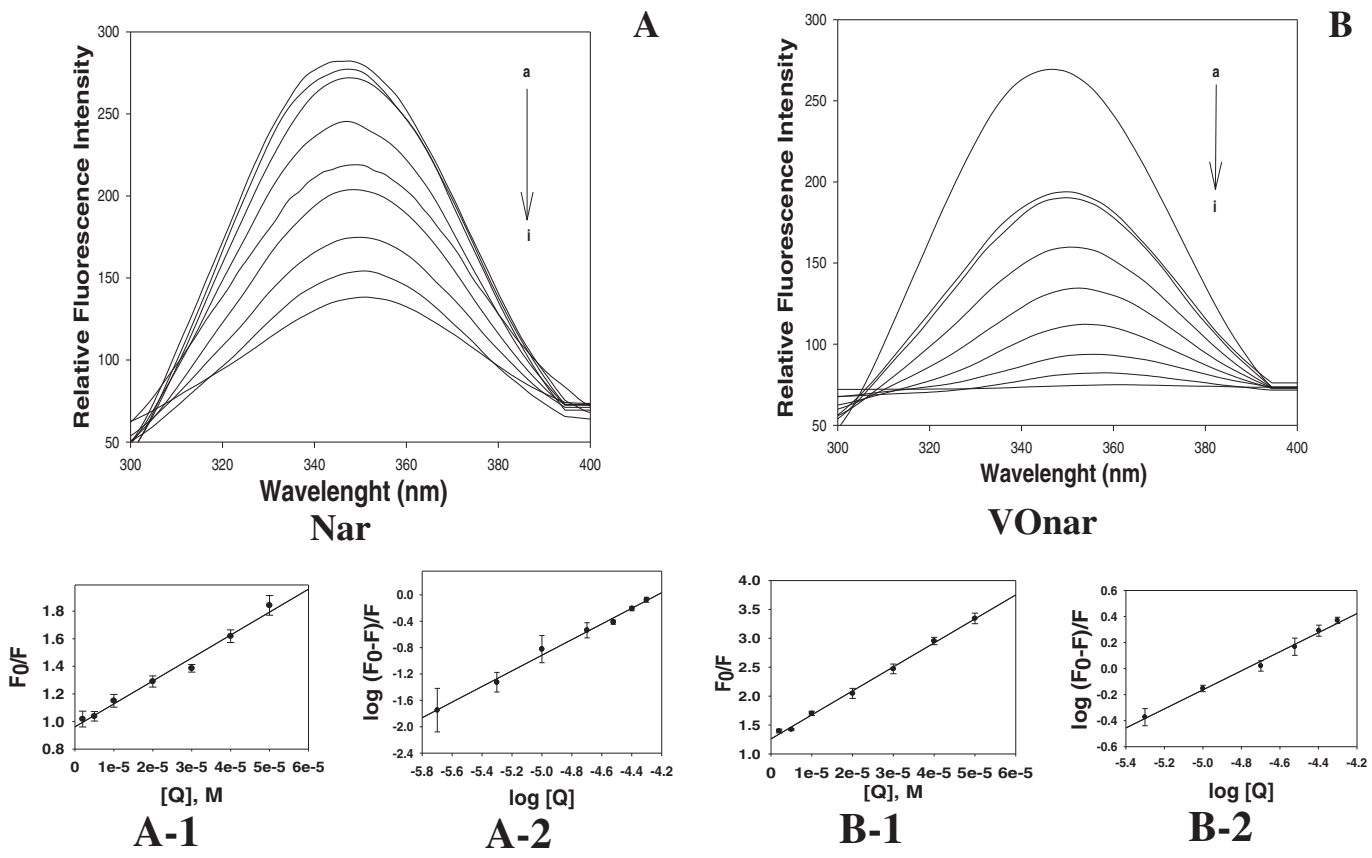


**Fig. 10.** Fluorescence quenching experiments for naringenin (A) and VOnar (B). Spectra of solutions of BSA at a fixed concentration (6 μM) and different concentrations of each of the compounds at 298 K. Concentration range: (a) BSA 6 μM (basal) and BSA 6 μM with successive addition of the compounds, (b) 2 μM, (c) 5 μM, (d) 10 μM, (e) 20 μM, (f) 30 μM, (g) 40 μM, (h) 50 μM, (i) 100 μM. Stern–Volmer plot of the fluorescence quenching of BSA with different concentrations of naringenin: naringenin-BSA (A-1) and VOnar-BSA (B-1) systems. Plot of log $(F_0–F)/F$ *vs.* log [Q] naringenin-BSA (A-2) and VOnar-BSA systems (B-2). Results represent the mean values ± the standard error of the mean (SEM) from three separate experiments.

intensity indicating that both compounds interacted with BSA producing a bathochromic shift (red shift) in the maximum emission wavelength of BSA (from 346 to 351 nm and from 346 to 357 nm, respectively). The red shift may probably be due to the loss of the compact structure of hydrophobic sub-domain where tryptophan was placed [61]. The effect of free $V(IV)O^{2+}$ cation on the fluorescence of BSA showed that the increasing concentrations of $V(IV)O^{2+}$ scarcely changed the fluorescence intensity of BSA. It had a slight blue-shift of BSA fluorescence emission maximum wavelength when the solution of $V(IV)O^{2+}$ was added, leading to a 10% quenching of fluorescence at 100 μM and suggesting that the binding is possibly associated with changes in the dielectric environment of at least one of the two indole rings in BSA [62].

The fluorescence quenching may be dynamic, resulting from the diffusive encounter between quencher and fluorophore during the life time of the excited state, or static, resulting from the formation of a fluorescent ground-state complex (fluorophore-quencher). Dynamic quenching of fluorescence is described by the Stern–Volmer equation (Eq. (2)):

$$F_o/F = 1 + Ksv[Q] \quad (2)$$

In this equation, $F_0$ and F are the fluorescence intensities in the absence and presence of the quencher, respectively. [Q] is the quencher concentration and Ksv is the Stern–Volmer quenching constant [62]. Taking into account the well known relationship between the quenching rate constant of the biomolecule $K_q$ and the dynamic quenching constant $K_{sv}$ ($K_q = K_{sv}/\tau_0$, where $\tau_0$ is the average lifetime of the biomolecule without quencher), and in consideration that the fluorescence lifetime of the biopolymer is $10^{-8}$ s, $K_q$ can be calculated using this equation. It is important to note that the Stern–Volmer curve should be linear for both, dynamic and static quenching. In the linear range of the Stern–Volmer curves (Figs. 10A-1, 10B-1), all the average Kq was far greater than $2.0 \times 10^{10}$ $M^{-1}$ $s^{-1}$ (Table 4), indicating that all the fluorescence quenching was probably originated from the formation of compound-BSA complex for static quenching procedure.

The value of the binding constant, Ka, is significant to understand the distribution of the drug in plasma [63]. The binding constant and the binding sites (n) can be calculated by the double-logarithm equation, Eq. (3):

$$\log((F_o - F)/F) = \log Ka + n\log[Q] \quad (3)$$

where Ka and n are the binding constant to a site and the number of binding sites per BSA, respectively. The values for Ka and n per BSA acquired in the absence and presence of metal ions from the plots in Figs. 10A–2 and 10B-2 are listed in Table 4. Both Ka and n values for

**Table 4**
Fluorescence experiments. Stern–Volmer constant (Ksv), quenching rate constant (Kq), binding constant (Ka) and n binding sites for the interaction of naringenin and VOnar (Concentration range: 2–100 μM) with BSA (6 μM) in Tris–HCl (0.1 M, pH 7.4). Results represent the mean values ± standard error of the mean (SEM) from three separate experiments.

| Compound | Ksv ($M^{-1}$) ($\times 10^4$) | Kq ($M^{-1}$ $s^{-1}$) ($\times 10^{12}$) | Ka ($M^{-1}$) ($\times 10^4$) | n |
|---|---|---|---|---|
| Naringenin | 1.66 ± 0.08 | 1.66 ± 0.08 | 10.20 ± 0.30 | 1.18 ± 0.07 |
| VOnar | 4.15 ± 0.30 | 4.15 ± 0.30 | 0.31 ± 0.01 | 0.73 ± 0.03 |

naringenin ($1.02 \times 10^5\ M^{-1}$ and 1.18, respectively) agreed with those of literature [64]. The different values obtained for the complex clearly indicate that under similar experimental conditions, the interaction of the VOnar complex with BSA differs markedly from that of the simple oxidovanadium(IV) cation and the ligand. The lower value for the binding constant of the complex ($Ka = 3.15 \times 10^3\ M^{-1}$) compared with the naringenin could be probably associated with the steric hindrance of the large molecular size of VOnar complex. Therefore, it has been demonstrated that the metal complex shows weaker binding to the protein and this kind of affinity probably will produce the promptly release of the complex from the plasma protein reservoir. As a result, it can be assumed that this complex may be stable in biological systems and may be carried by albumin.

## 4. Conclusions

In summary, the new polymeric complex of naringenin with the oxidovanadium(IV) cation has been found to be a more effective antioxidant than naringenin and an antiproliferative agent against A549 and MDAMB231 and SKBr3 human cancer cell lines, being this effect more prominent in the latter lines. Mechanistic investigation on the anticancer activity in the breast cancer cell lines revealed that naringenin produced only cellular membrane damage among the tested parameters. The anticancer potential of VOnar has been supported by the evidence provided in the present study, including lactate dehydrogenase leakage, oxygen reactive species generation, loss in mitochondrial membrane potential, activation of caspase 3/7 and DNA damage. The results confirmed the involvement of intrinsic pathways in induced apoptosis in both cellular types and the selective effects of VOnar depended on the basal antioxidant machinery of each cell. Complexation influenced the binding affinity to bovine serum albumin of the flavonoid. A steric hindrance may be the cause of the decrease of the binding affinity with protein of VOnar and this effect can be correlated to its bioavalability.

## Abbreviations

| | |
|---|---|
| ABTS | 2,2′-Azinobis(3-ethylbenzothiazoline-6-sulfonic acid) diammonium salt |
| BSA | bovine serum albumin |
| Crystal violet | tris(4-(dimethylamino)phenyl)methylium chloride |
| DPPH• | 1,1-diphenyl-2-picrylhydrazyl |
| FBS | fetal bovine serum |
| H2AX | subtype of H2A histone |
| DCFH-DA | 2′,7′-dichlorodihydrofluorescein diacetate |
| GSH | glutathione |
| LDH | lactate dehydrogenase |
| MTT | 3-(4,5-dimethylthiazol-2-yl)-2,5diphenyltetrazolium bromide |
| PBS | phosphate-buffered saline |
| ROIs | regions-of-interest |
| ROS | reactive oxygen species |
| RPMI medium | Roswell Park Memorial Institute culture medium |
| TMRM | tetramethyl rhodamine methyl ester |
| VOnar | $[V^{IV}O(nar)_2]\cdot 2H_2O$ |

## Acknowledgments

This work was supported by UNLP, CONICET, CICPBA (PICyT 813/13) and ANPCyT (PICT-2013-0569), Argentina. EGF, LGN are research fellows of CONICET. PAMW is a research fellow of CICPBA, Argentina. MSI is a fellowship holder from CONICET. Convenio de vinculación tecnológica. Expte-CONICET-004200/13; TQ1/13.

## References

[1] S. Selvaraj, S. Krishnaswamy, V. Devashya, S. Sethuraman, U.M. Krishnan, Med. Res. Rev. 34 (2014) 677–702.
[2] A. Mohan, S. Narayanan, S. Sethuraman, U.M. Krishnan, Anticancer Agents Med Chem. 13 (2013) 281–295.
[3] E.G. Ferrer, P.A.M. Williams, Modification of flavonoid structure by oxovanadium(IV) complexation. Biological effects, in: K. Yamane, Y. Kato (Eds.), Handbook on Flavonoids: Dietary Sources, Properties and Health Benefits, Nova Science Publishers, Inc, New York 2011, pp. 145–190.
[4] E. Tripoli, M.L. Guardia, S. Giammanco, D.D. Majo, M. Giammanco, Food Chem. 104 (2007) 466–479.
[5] F.V. So, N. Guthrie, A.F. Chambers, M. Moussa, K.K. Carroll, Nutr. Cancer 26 (1996) 167–181.
[6] R.M.S. Pereira, N.E.D. Andrades, N. Paulino, A.C.H.F. Sawaya, M.N. Eberlin, M.C. Marcucci, G. Marino Favero, E.M. Novak, S.P. Bydlowski, Molecules 12 (2007) 1352–1366.
[7] H.L. Wang, Z.Y. Yang, B. Wang, Transit. Met. Chem. 31 (2006) 470–474.
[8] M. Tan, J. Zhu, Y. Pan, Z. Chen, H. Liang, H. Liu, H. Wang, Bioinorg. Chem. Appl. 2009 (2009). 1–9, http://dx.doi.org/10.1155/2009/347872 (Hindawi Publishing Corporation).
[9] A.S. Tracey, G.R. Willsky, E.S. Takeuchi, Vanadium: chemistry, biochemistry, Pharmacology and Practical Applications, CRC Press, Boca Ratón, 2007.
[10] L.G. Naso, M. Valcarcel, P. Villacé, M.I Roura-Ferrer, C. Salado, E.G. Ferrer, P.A.M. Williams, New J. Chem. 38 (2014) 2414–2421.
[11] E.G. Ferrer, M.V. Salinas, M.J. Correa, L.G. Naso, D.A. Barrio, S.B. Etcheverry, L. Lezama, T. Rojo, P.A.M. Williams, J. Biol. Inorg. Chem. 11 (2006) 791–801.
[12] L.G. Naso, E.G. Ferrer, L. Lezama, T. Rojo, S.B. Etcheverry, P.A.M. Williams, J. Biol. Inorg. Chem. 15 (2010) 889–902.
[13] L.G. Naso, E.G. Ferrer, N. Butenko, I. Cavaco, L. Lezama, T. Rojo, S.B. Etcheverry, P.A.M. Williams, J. Biol. Inorg. Chem. 16 (2011) 653–668.
[14] L. Naso, L. Lezama, T. Rojo, S.B. Etcheverry, M. Valcarcel, M. Roura, C. Salado, E. Ferrer, P.A.M. Williams, Chem. Biol. Interact. 206 (2013) 289–301.
[15] M. Onishi, Photometric Determination of Traces of Metals, 4th ed Wiley, New York, 1998. part II.
[16] J. Pasán, J. Sanchiz, C. Ruiz-Pérez, F. Lloret, M. Julve, Eur. J. Inorg. Chem. (2004) 4081–4090.
[17] M. Jabbari, F. Gharib, J. Mol. Liq. 168 (2012) 36–41.
[18] M. Rajendran, R. Ravichandran, D. Devapiriam, Int. J. Comput. Appl. 77 (2013) 18–25.
[19] A.A. Farajtabar, F. Gharib, Chem. Pap. 67 (2013) 538–545.
[20] C.H. Ríos Martínez, C. Dardonville, Med. Chem. Lett. 4 (2013) 142–145.
[21] D. Sanna, V. Ugone, G. Lubinu, G. Micera, E. Garribba, J. Inorg. Biochem. 140 (2014) 173–184.
[22] G. Sichel, C. Corsaro, M. Scalia, A.J. Di Billio, R.P. Bonomo, Free Radic. Biol. Med. 11 (1991) 1–8.
[23] O. Benavente-García, J. Castillo, F.R. Marin, A. Ortuño, J.A. Del Río, J. Agric. Food Chem. 45 (1997) 4505–4515.
[24] S. Burda, W. Oleszek, J. Agric. Food Chem. 49 (2001) 2774–2779.
[25] M. Ajay, H.M. Cheng, A.M. Mustafa, M.R. Mustafa, Malays. J. Sci. 24 (2005) 187–190.
[26] K.L. Khanduja, A. Bhardwaj, Indian J. Biochem. Biophys. 40 (2003) 416–422.
[27] K.E. Heim, A.R. Tagliaferro, D.J. Bobilya, J. Nutr. Biochem. 13 (2002) 572–584.
[28] R. Re, N. Pellegrini, A. Proteggente, A. Pannala, M. Yang, C. Rice-Evans, Free Radic. Biol. Med. 26 (1999) 1231–1237.
[29] P.G. Pietta, J. Nat. Prod. 63 (2000) 1035–1042.
[30] J. Tabart, C. Kevers, J. Pincemail, J.O. Defraigne, J. Dommes, Food Chem. 113 (2009) 1226–1233.
[31] M.K. Johnson, G. Loo, Mutat. Res. 459 (2000) 211–218.
[32] P. Cos, L. Ying, M. Calomme, J.P. Hu, K. Cimanga, B.V. Poel, L. Pieters, A.J. Vlietinck, D.V. Berghe, J. Nat. Prod. 61 (1998) 71–76.
[33] F. Orallo, M. Camiña, E. Álvarez, H. Basaran, C. Lugnier, Planta Med. 71 (2005) 99–107.
[34] M. Cavia-Saiz, M.D. Busto, M. Concepción, P. Izquierdo, N. Ortega, M. Perez-Mateos, P. Muñiz, J. Sci. Food Agric. 90 (2010) 1238–1244.
[35] W.Y. Huang, K. Majumder, J. Wu, Food Chem. 123 (2010) 635–641.
[36] Y. Mino, T. Ishida, N. Ota, M. Inoue, K. Nomoto, H. Yoshioka, T. Takemoto, Y. Sugiura, H. Tanaka, Inorg. Chem. 20 (1981) 3440–3444.
[37] S. Rafat, H.J. Cilurd, P. Cillard, Phytochemistry 26 (1987) 2489–2491.
[38] C.D. Hapner, P. Deuster, Y. Chen, Chem. Biol. Interact. 186 (2010) 275–279.
[39] S.A. Mir, A.S. Bhat, A.A. Ahangar, Int. J. Pharm. Tech. Res. 6 (2014) 759–768.
[40] C.A. RiceEvans, N.J. Miller, P.G. Bolwell, P.M. Bramley, J.B. Pridham, Free Radic. Res. 22 (1995) 375–383.
[41] P. Cos, L. Ying, M. Calomme, J.P. Hu, K. Cimanga, B. Van Poel, L. Pieters, A.J. Vlietinck, D. Vanden Berghe, J. Nat. Prod. 61 (1998) 71–76.
[42] F. Li, S. Awale, Y. Tezuka, S. Kadota, Bioorg. Med. Chem. 16 (2008) 5434–5440.
[43] J. Manthey, N. Guthrie, J. Agric. Food Chem. 50 (2002) 5837–5843.
[44] E. Lee, Y. Kang, H. Choi, G. Kang, J. Kim, B. Kim, Y. Han, S. Nah, H. Paik, Y. Park, S. Cho, Biol. Pharm. Bull. 30 (2007) 2394–2398.
[45] K. Chidambara Murthy, J. Kim, A. Vikram, B. Patil, Food Chem. 132 (2012) 27–34.
[46] J.B. White, J. Beckford, S. Yadegarynia, N. Ngo, T. Lialiutska, M. D'Alarcao, Food Chem. 131 (2012) 1453–1459.
[47] S. Yadegaryania, A. Pham, A. Ng, D. Nguyen, T. Lialiutska, A. Bortolazzo, V. Sivryuk, M. Bremer, J.B. White, Nat. Prod. Commun. 7 (2012) 1295–1304.
[48] W. Lee, W. Chen, C. Wang, W. Lin, T. Tseng, Toxicol. Appl. Pharmacol. 226 (2008) 178–191.
[49] S. Kanno, A. Tomizawa, T. Hiura, Y. Osanai, A. Shouji, M. Ujibe, T. Ohtake, K. Kimura, M. Ishikawa, Biol. Pharm. Bull. 28 (2005) 527–530.

[50] B. Wang, Z. Yang, Q. Wang, T. Cai, P. Crewdson, Bioorg. Med. Chem. 14 (2006) 1880–1888.
[51] Q. Wang, T. Liu, Y. Fu, K. Wang, X. Yang, J. Biol. Inorg. Chem. 15 (2010) 1087–1097.
[52] S. Burrow, G. Valet, Eur. J. Cell Biol. 43 (1987) 128–133.
[53] A. Cheng, T. Huang, C. Lai, M. Pan, Eur. J. Pharmacol. 509 (2005) 1–10.
[54] D.R. McIlwain, T. Berger, T.W. Mak, Cold Spring Harb. Perspect. Biol. 5 (2013) a008656.
[55] M. Podhorecka, A. Skladanowski, P. Bozko, J. Nucleic Acids (2011) 1–9 (2010).
[56] M.R. Webb, S.E. Ebeler, Biochem. J. 384 (2004) 527–541.
[57] R. Prabhakaran, P. Kalaivani, R. Huang, P. Poornima, V. Vijaya Padma, F. Dallemer, K. Natarajan, J. Biol. Inorg. Chem. 18 (2013) 233–247.
[58] T. Noda, R. Iwakiri, K. Fujimoto, T.Y. Aw, FASEB J. 15 (2001) 2131–2139.
[59] S. Yadegarynia, A. Pham, A. Nga, D. Nguyen, T. Lialiutsk, A. Bortolazzo, V. Sivryuk, M. Bremer, J.B. White, Nat. Prod. Commun. 9 (2014) 597–606.
[60] L.G. Naso, M. Valcarcel, M. Roura-Ferrer, D. Kortazar, C. Salado, L. Lezama, T. Rojo, A.C. González-Baró, P.A.M. Williams, E.G. Ferrer, J. Inorg. Biochem. 135 (2014) 86–99.
[61] P.B. Kandagal, S.S. Kalanur, D.H. Manjunatha, J. Seetharamappa, J. Pharm. Biomed. Anal. 47 (2008) 260–267.
[62] S. Bi, L. Yan, B. Pang, Y. Wang, J. Lumin. 132 (2012) 132–140.
[63] Y. Zhang, S. Shi, X. Sun, X. Xiong, M. Peng, J. Inorg. Biochem. 105 (2011) 1529–1537.
[64] J. Shi, H. Cao, Braz. J. Pharmacogn. 21 (2011) 594–600.